Acta Crystallographica Section D
**Biological Crystallography**
ISSN 0907-4449

# Structures of *Enterovirus 71* 3C proteinase (strain E2004104-TW-CDC) and its complex with rupintrivir

**Caiming Wu,[a]‡ Qixu Cai,[a]‡ Chen Chen,[a] Ning Li,[b] Xuanjia Peng,[b] Yaxian Cai,[b] Ke Yin,[b] Xinsheng Chen,[b] Xiaolong Wang,[a] Rongfu Zhang,[a] Lijie Liu,[a] Shuhui Chen,[b] Jian Li[b]* and Tianwei Lin[a]***

[a]State Key Laboratory of Cellular Stress Biology, School of Life Sciences, Xiamen University, Xiamen, Fujian 361102, People's Republic of China, and [b]State Key Laboratory on Lead Compound Research, WuXi AppTech Co. Ltd, Shanghai 200131, People's Republic of China

‡ These authors contributed equally to this work.

Correspondence e-mail: jian_li@wuxiapptec.com, twlin@xmu.edu.cn



Received 11 December 2012
Accepted 28 January 2013

**PDB References:** *Enterovirus 71* 3C proteinase, 4ghq; *Enterovirus 71* 3C proteinase in complex with AG7088, 4ght

The crystal structure of 3C proteinase ($3C^{pro}$) from *Enterovirus 71* (EV71) was determined in space group $C222_1$ to 2.2 Å resolution. The fold was similar to that of $3C^{pro}$ from other picornaviruses, but the difference in the $\beta$-ribbon reported in a previous structure was not observed. This $\beta$-ribbon was folded over the substrate-binding cleft and constituted part of the essential binding sites for interaction with the substrate. The structure of its complex with rupintrivir (AG7088), a peptidomimetic inhibitor, was also characterized in space group $P2_12_12_1$ to 1.96 Å resolution. The inhibitor was accommodated without any spatial hindrance despite the more constricted binding site; this was confirmed by functional assays, in which the inhibitor showed comparable potency towards EV71 $3C^{pro}$ and human rhinovirus $3C^{pro}$, which is the target that rupintrivir was designed against.

## 1. Introduction

Enteroviruses belong to the *Picornaviridae* (Racaniello, 2006) and include a large number of clinically significant pathogens. Enteroviruses such as polioviruses and coxsackieviruses have a long history of causing severe suffering and death in humans, and the outbreaks of hand, foot and mouth disease (HFMD) caused by *Enterovirus 71* (EV71) and coxsackieviruses in recent years highlight the importance of controlling and treating the associated diseases. The large number of serotypes represents a substantial obstacle to curtailing infection using the vaccine strategy, but the development of antivirals against high-value therapeutic targets with commonality across the serotypes is an effective measure.

Enteroviruses are icosahedral viruses with single-stranded and positive-sense RNA genomes. After entry into the cell, their replication starts with the translation of a polyprotein precursor from the monocistronic genome, which is subsequently processed into mature proteins by virally encoded proteinases (Racaniello, 2006). All but one of the proteolytic processes depend on the activity of 3C proteinase ($3C^{pro}$). Besides being an essential component in the life cycle of enteroviruses, $3C^{pro}$ also plays crucial roles in controlling the cellular replication machinery as well as in evading and suppressing the host defence mechanisms (Yang *et al.*, 2007; Weng *et al.*, 2009).

The essential roles of $3C^{pro}$ in the viral life cycle make it an important therapeutic target. It is of significance to characterize its structures to high resolution for the structure-based development of therapeutics. The crystal structure of EV71 $3C^{pro}$ has previously been determined to 3 Å resolution and a unique conformation of a $\beta$-ribbon was identified (Cui *et*

*al.*, 2011). In addition, the S2 substrate-binding site was shown to be too constricted for optimal interaction with the peptidomimetic inhibitor rupintrivir designed for human rhinovirus (HRV) 3C$^{pro}$ (Lu *et al.*, 2011). Here, the crystal structures of EV71 3C$^{pro}$ and its complex with rupintrivir were determined in different space groups. The conformation of the $\beta$-ribbon was the same as those in all other picornavirus 3C$^{pro}$ structures and constituted an essential part of the substrate-binding cleft, but differed from that in the previous EV71 3C$^{pro}$ structure (Cui *et al.*, 2011). Despite the slightly smaller S2 site, the site was sufficiently large to accommodate the corresponding interacting moiety of rupintrivir, which was corroborated by enzymatic and cell-based assays. The difference in rupintrivir binding to 3C$^{pro}$ from HRV and EV71 was attributed to a different distribution of charged groups in the S2 site.

## 2. Methods

### 2.1. Protein expression and purification

The cDNA encoding EV71 3C$^{pro}$ (residues 1549–1731 of the polyprotein of EV71 strain E2004104-TW-CDC; GenBank Accession No. EF373576) was synthesized (Sangon, Shanghai) and cloned into the *Nco*I and *Xho*I sites of pET28a expression plasmid (Novagen). *E. coli* strain BL21(DE3) cells carrying the plasmid were cultured in LB medium with kanamycin (50 µg ml$^{-1}$) at 310 K. Protein expression was induced using 0.5 m*M* isopropyl $\beta$-D-1-thiogalactoside for 12 h at 293 K after the $OD_{600\,nm}$ of the culture had reached 0.8. The *E. coli* cells were harvested by centrifugation at 4500*g* for 30 min with a Beckman–Coulter rotor (JS4.2). The cells were lysed by sonication in 25 m*M* Tris–HCl pH 7.5, 150 m*M* NaCl and the lysate was clarified by centrifugation at 30 000*g* with a Beckman–Coulter rotor (JA30.50 Ti) for 40 min. The supernatant was loaded onto an Ni–NTA column and the resin was washed with 25 m*M* Tris–HCl pH 7.5, 150 m*M* NaCl, 20 m*M* imidazole. The protein was eluted with 25 m*M* Tris–HCl pH 7.5, 150 m*M* NaCl, 300 m*M* imidazole. The buffer was exchanged to 25 m*M* Tris–HCl pH 7.5 in a Centricon centrifugal filter unit (MWCO 10 000) and the protein was further purified on a DEAE column by collecting the flowthrough. The protein was stored in 25 m*M* Tris–HCl pH 8.0, 150 m*M* NaCl, 1 m*M* TCEP at 277 K.

### 2.2. Crystallization and structure determination

Crystals of EV71 3C$^{pro}$ were obtained by the hanging-drop vapour-diffusion method and the drops were prepared using a 1:1 mixture of EV71 3C$^{pro}$ (12 mg ml$^{-1}$) and reservoir solution consisting of 100 m*M* Tris–HCl pH 8.5, 25% PEG 4000, 0.8 *M* lithium chloride. Crystals suitable for data collection were obtained after about one week at 289 K.

The inhibitor complex was prepared by mixing the protease and the compound in a 1:5 molar ratio and incubating at 277 K overnight. The conditions used for cocrystallization were basically the same as those used for the protein alone.

The crystals were flash-cooled to 100 K and X-ray diffraction data for EV71 3C$^{pro}$ were collected on beamline BL17U1 at Shanghai Synchrotron Radiation Facility (SSRF) using an ADSC Quantum 315r CCD detector and were processed using the *HKL*-2000 package (Otwinowski & Minor, 1997). The data for the rupintrivir complex were collected using an in-house X-ray facility equipped with a Rigaku X-ray generator (MicroMax-007 HF) and a MAR345dtb detector and were processed using the *automar* package from MAR Research GmbH.

The structure of EV71 3C$^{pro}$ was solved by molecular replacement using the program *Phaser* (McCoy *et al.*, 2007). The coordinates of poliovirus 3C$^{pro}$ (PDB entry 1l1n; Mosimann *et al.*, 1997) were used as the search model. Manual model building and refinement were performed with *Coot* (Emsley *et al.*, 2010) and *REFMAC*5 (Murshudov *et al.*, 1997,

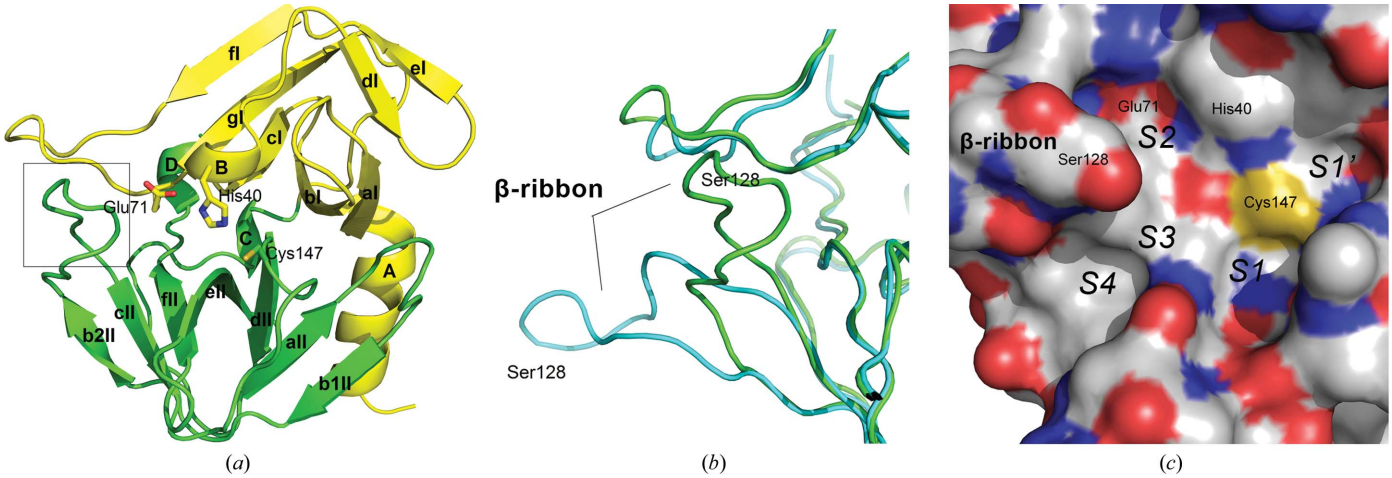


(*a*) (*b*) (*c*)

**Figure 1**
The structure of EV71 3C$^{pro}$. (*a*) Ribbon diagram of the EV71 3C$^{pro}$ structure. The N-terminal domain is shown in yellow and the C-terminal domain is shown in green. The catalytic residues are shown as sticks. The area with a different structure from that reported previously by Cui *et al.* (2011) is boxed. (*b*) Differences in structure. The current structure is shown in green while the previous structure as reported by Cui *et al.* (2011) is shown in cyan. The $\beta$-ribbons are indicated. (*c*) Surface rendering of the substrate-binding cleft and active site. The $\beta$-ribbon forms an essential part of the S2, S3 and S4 sites. The nomenclature for the substrate-binding sites is as defined by Schechter & Berger (1967).

2011; Winn *et al.*, 2011). The refined 3C$^{pro}$ structure was used as the search model to determine the structure of the complex. The compound library file was generated using *JLigand* (Lebedev *et al.*, 2012). The figures were produced using *PyMOL* (Schrödinger).

### 2.3. Enzymatic activity assay

The substrate was derived from the 3B–3C junction in the polyprotein with a FRET pair attached at the two termini. The sequence was Dacyl-KRTATVQGPSLDFE-Edans. The assay was carried out with 5 µ*M* enzyme in 100 µl 50 m*M* Tris–HCl pH 7.0, 100 m*M* NaCl, 1 m*M* TCEP. The cleavage was monitored using a Cary Eclipse fluorescence spectrophotometer (Varian). The excitation wavelength was 340 nm and the emission wavelength was 495 nm. The initial velocity was used to calculate $IC_{50}$ with the *GraphPad Prism* computer program.

### 2.4. Cell-based activity assay

Human embryonic rhabdomyosarcoma (RD) cells were seeded in a 96-well cell-culture plate (8000 cells per well) in Dulbecco's Modified Eagle's Medium (DMEM) with 2% foetal bovine serum (FBS). The cells were pre-incubated overnight in a 5% $CO_2$ incubator at 310 K. The virus (EV71/Shenzhen/120F1/09 at 100× $TCID_{50}$) and the chemical compounds in DMSO were added to the cells and incubated at 310 K for 72 h. The final concentration of DMSO in each well was 1%. CCK-8 was added to each well at the end of incubation to determine the cell viability. The optical density in each well was measured at 450 nm. The concentration of compound required to reduce virus-induced cell death by 50% was defined as the $EC_{50}$.

## 3. Results and discussion

### 3.1. Structures of EV71 3C$^{pro}$

The crystal structure of EV71 3C$^{pro}$ (strain E2004104-TW-CDC) was determined to 2.2 Å resolution in space group $C222_1$ with well defined electron density for residues 1–180. Its two $\beta$-barrel domains adopt a chymotrypsin-like fold, which is conserved in all other picornavirus 3C$^{pro}$ structures, and each domain consists of two $\alpha$-helices and seven antiparallel $\beta$-strands (Fig. 1*a* and Table 1). The substrate-binding cleft is located between the domains, with a Cys-His-Glu catalytic triad in a similar conformation to the Ser-His-Asp triad found in most serine proteases.

The sequence between the $\beta$b2II and $\beta$cII strands is folded over the substrate-binding cleft as a conserved $\beta$-ribbon in this EV71 3C$^{pro}$ structure (Figs. 1*a* and 1*b*); this is similar to all other picornavirus 3C$^{pro}$ structures but differs from a previous EV71 3C$^{pro}$ structure in a different space group (Fig. 1*b*; Cui *et al.*, 2011). The EV71 proteins used in the two separate studies are highly similar, with an overall sequence identify of 99% and no sequence differences in the $\beta$-ribbon and its surrounding residues. In the EV71 3C$^{pro}$ structure the $\beta$-ribbon constitutes an essential component in the formation of the substrate-binding cleft, folding over the substrate-binding sites like a peninsula with S2, S3 and S4 on its three

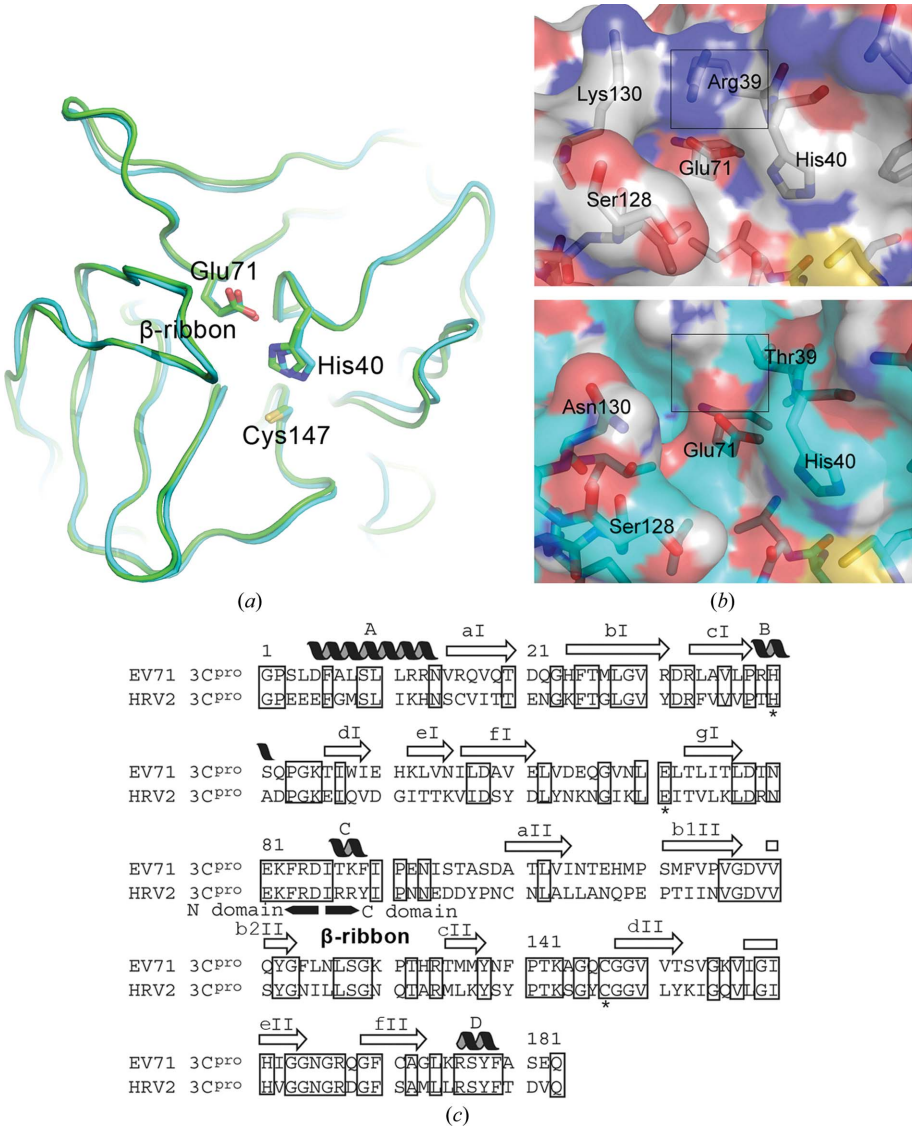


**Figure 2**
The active sites of EV71 and HRV 3C$^{pro}$. (*a*) Superposition of the active sites of EV71 and HRV 3C$^{pro}$. The chain trace of EV71 3C$^{pro}$ is shown in green, while that of HRV 3C$^{pro}$ is shown in cyan. (*b*) S2 sites of EV71 3C$^{pro}$ (top) and HRV2 3C$^{pro}$. The larger side chains of Lys130 and Arg39 make the S2 site in EV71 3C$^{pro}$ smaller, but provide additional charge. (*c*) Sequence alignment of EV71 3C$^{pro}$ and HRV2 3C$^{pro}$. The secondary structures are shown. Identical residues are boxed. The identity between the two sequences is 44.3%. The active residues are indicated by asterisks below.

**Table 1**
Data-collection and refinement statistics.

Values in parentheses are for the highest resolution shell.

| | $3C^{pro}$ | Rupintrivir complex |
|---|---|---|
| Data collection | | |
| Space group | $C222_1$ | $P2_12_12_1$ |
| Unit-cell parameters | | |
| $a$ (Å) | 64.559 | 63.885 |
| $b$ (Å) | 63.374 | 64.254 |
| $c$ (Å) | 75.282 | 75.811 |
| Resolution (Å) | 50–2.20 (2.24–2.20) | 50–1.96 (2.03–1.96) |
| $R_{merge}$ | 0.117 (0.540) | 0.111 (0.4926) |
| $\langle I/\sigma(I)\rangle$ | 17.5 (3.0) | 8.5 (2.0) |
| Completeness (%) | 100 (100) | 99.9 (100) |
| Multiplicity | 7.0 (6.9) | 6.47 (6.56) |
| Refinement | | |
| Resolution (Å) | 2.20 | 1.96 |
| No. of reflections | 7750 | 21832 |
| $R_{work}/R_{free}$ | 0.186/0.277 | 0.205/0.279 |
| No. of atoms | | |
| Protein | 1393 | 2786 |
| Ligand/ion | 0 | 86 |
| Water | 94 | 194 |
| $B$ factors (Å$^2$) | | |
| Protein | 29.6 | 25.6 |
| Ligand/ion | 0 | 31.8 |
| Water | 33 | 30.3 |
| Ramachandran statistics† (%) | | |
| Most favoured region | 96.65 | 94.69 |
| Allowed regions | 3.35 | 4.75 |
| Outliers | 0 | 0.56 |
| R.m.s. deviations | | |
| Bond lengths (Å) | 0.013 | 0.015 |
| Bond angles (°) | 1.60 | 1.91 |

† The Ramachandran statistics were calculated by *Coot* (Emsley *et al.*, 2010).

peripheries (Fig. 1*c*). The $B$ factors are high in the $\beta$-ribbon. Compared with an average $B$ factor of 25 Å$^2$ for the full structure (Table 1), the $B$ factor for the C$^{\alpha}$ atom of Ser128 at the apical tip of the $\beta$-ribbon is about 90 Å$^2$, which is indicative of high flexibility. This high flexibility would be desirable for structural adjustment to the binding of substrates, as has been demonstrated in the structures of complexes between the substrate and $3C^{pro}$ from *Hepatitis A virus* and *Foot and mouth disease virus* (FMDV) (Yin *et al.*, 2006; Zunszain *et al.*, 2010), but it would also make the sequence malleable for distortion once it is involved in intermolecular contacts in the absence of an inhibitor or a substrate. In the previous EV71 $3C^{pro}$ structure the $\beta$-ribbon sequence was indeed involved in an intermolecular interaction owing to crystal packing (Cui *et al.*, 2011), which is likely to induce another conformation with no physiological relevance.

This structural discrepancy between different crystal forms of EV71 $3C^{pro}$ is also reminiscent of a previous finding that was convincingly demonstrated by structural and mutational studies of $3C^{pro}$ from FMDV (Birtley *et al.*, 2005; Sweeney *et al.*, 2007; Zunszain *et al.*, 2010). The apical tip residues of the FMDV $3C^{pro}$ $\beta$-ribbon have a high degree of flexibility with high $B$ factors (Sweeney *et al.*, 2007) and could adjust to the interaction with substrate (Zunszain *et al.*, 2010). However, the structure of the flexible $\beta$-ribbon in FMDV $3C^{pro}$ was altered to a non-native conformation without a bound inhibitor or substrate when it was involved in an intermolecular contact in the crystal (Birtley *et al.*, 2005; Sweeney *et al.*, 2007). Since the $\beta$-ribbon in this EV71 $3C^{pro}$ structure forms an essential part of the S2, S3 and S4 sites (Fig. 1*c*), which is similar to all other $\beta$-ribbons in various picornavirus $3C^{pro}$ structures, and is not involved in crystal packing, its conformation should represent the native structure. As the $\beta$-ribbon was involved in crystal packing in the previous crystal and was folded away from the substrate-binding cleft (Cui *et al.*, 2011), which would result in a nonfunctional enzyme with a distorted substrate-binding cleft, it supports the contention that the 'different conformation' observed in the previous EV71 $3C^{pro}$ structure was a corollary of crystalline interactions between the protease molecules and was not native, which is supported by the findings from the structural studies of FMDV $3C^{pro}$ (Birtley *et al.*, 2005; Sweeney *et al.*, 2007; Zunszain *et al.*, 2010).

### 3.2. Active site of EV71 $3C^{pro}$

The substrate-binding cleft of EV71 $3C^{pro}$ is highly similar to that of human rhinovirus 2 (HRV2), with a well superposed

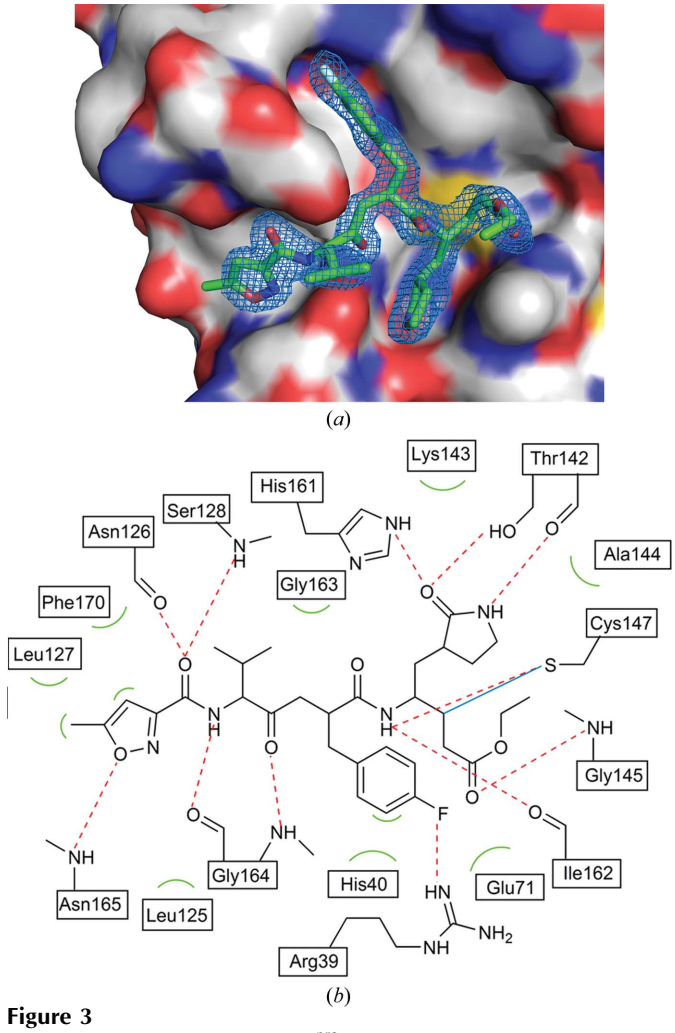


**Figure 3**
Interaction between EV71 $3C^{pro}$ and rupintrivir. (*a*) Binding of rupintrivir. The enzyme is shown with surface rendering and rupintrivir is shown as sticks with C atoms in green, O atoms in red and N atoms in blue. The electron density for rupintrivir is also shown. (*b*) Schematic diagram of the interactions between rupintrivir and EV71 $3C^{pro}$.

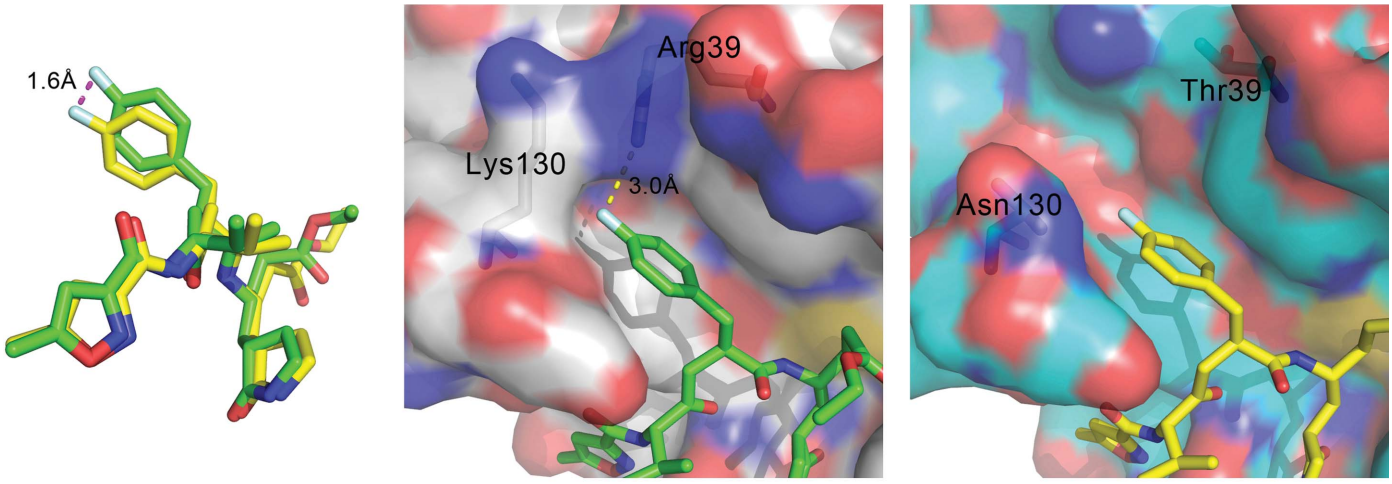


**Figure 4**
Different binding of rupintrivir to EV71 3C$^{pro}$ and HRV 3C$^{pro}$. (*a*) The slight difference in the position of rupintrivir binding to EV71 3C$^{pro}$ and HRV 3C$^{pro}$. In the stick model, the C atoms of rupintrivir bound to EV71 3C$^{pro}$ are shown in green, while those of that bound to HRV2 3C$^{pro}$ are shown in yellow. (*b*) The S2 site in EV71 3C$^{pro}$ is more confined but accommodates the fluorobenzene group without spatial constraints. The F atom interacts with Arg39. (*c*) Interaction at the S3 site of HRV2 3C$^{pro}$. With Asn130 and Thr39 forming part of the S2 site, instead of Lys130 and Arg39 as in EV71 3C$^{pro}$, the site is larger and less charged than that in EV71 3C$^{pro}$. The fluorobenzene group interacts in a slightly deeper position because of the lack of interaction such as that observed in EV71 3C$^{pro}$.

catalytic triad of residues His40, Glu71 and Cys147 (Figs. 2*a* and 2*b*), despite the sequence identity between the two being only about 44% (Fig. 2*c*). The S1′, active and S1 sites form a relatively shallow dent on the surface of the enzyme (Fig. 1*c*). The S2 site is a defined cavity with a distinct difference from the S2 site of HRV2 3C$^{pro}$, in which the larger Arg39 and Lys130 in EV71 3C$^{pro}$ compared with Thr39 and Asn130 in HRV2 3C$^{pro}$ make the S2 site in EV71 3C$^{pro}$ more confined and positively charged (Fig. 2*b*). The S3 and S4 sites are similar to those in HRV2 3C$^{pro}$.

### 3.3. Structure of the complex with rupintrivir

Rupintrivir is a peptidomimetic that targets HRV2 3C$^{pro}$ (Matthews *et al.*, 1999). The overall similarity in the active site and substrate-binding cleft suggests that the interaction of rupintrivir with EV71 3C$^{pro}$ should be as favourable as that with HRV2 3C$^{pro}$, with the possible exception of the S2 site. The structure of the complex between EV71 3C$^{pro}$ and rupintrivir was characterized (Table 1 and Fig. 3*a*). Unsurprisingly, the pattern of interaction is similar to that reported previously (Lu *et al.*, 2011; Wang *et al.*, 2011), albeit in a different space group (Fig. 3). Rupintrivir binds to EV71 3C$^{pro}$ *via* a network of hydrogen bonds and hydrophobic interactions (Fig. 3*b*). Detectable differences between the EV71 3C$^{pro}$–rupintrivir complex and HRV2 3C$^{pro}$–rupintrivir complex are found at the S1′ and S2 sites. The terminal atoms at S1′ point away from the site in the EV71 3C$^{pro}$–rupintrivir complex structure (Fig. 3*a*). The tip of the S2-interacting moiety of rupintrivir in EV71 3C$^{pro}$ was 1.6 Å from the interacting position in HRV2 3C$^{pro}$ (Fig. 4*a*; Lu *et al.*, 2011; Wang *et al.*, 2011). However, this difference in interaction is minor and, contrary to the previous report, does not appear to originate from the more confined S2 in EV71 3C$^{pro}$ as the fluorobenzene group is snugly accommodated at the site with no apparent spatial restrictions (Figs. 4*b* and 4*c*). The difference in interaction at the S2 sites between EV71 3C$^{pro}$ and HRV 3C$^{pro}$ might arise from the fact that the F atom interacts with the side chain of Arg39 in EV71 3C$^{pro}$ while there is no similar charged group in HRV 3C$^{pro}$ (Figs. 4*b* and 4*c*).

### 3.4. Potency of rupintrivir against EV71 3C$^{pro}$

Rupintrivir is a potent inhibitor of the activity of HRV2 3C$^{pro}$. The crystallographic analysis in this study shows only a minor difference in the interaction of rupintrivir with HRV 3C$^{pro}$ and EV71 3C$^{pro}$. This finding is corroborated by the functional assay of rupintrivir inhibition of EV71 3C$^{pro}$ enzymatic activity and EV71 replication. The $IC_{50}$ of rupintrivir was 1.67 µ*M* for EV71 3C$^{pro}$ enzymatic activity and the $EC_{50}$ of rupintrivir for EV71 infectivity was 41 n*M* in a cell-based activity assay. In comparison, the $EC_{50}$ of rupintrivir was 13 n*M* for HRV2 infectivity (Matthews *et al.*, 1999), with a mean value of 23 n*M* for 48 strains of rhinovirus (Thomson Reuters Drug Report; http://www.thomsonpharma.com). Taking into account that the measurements were performed in different systems, rupintrivir should have a similar potency towards both EV71 and HRV, supporting the notion that rupintrivir is also a potent inhibitor of EV71 3C$^{pro}$.

## 4. Conclusions

Since the 1970s, epidemics and outbreaks of HFMD have been spreading around the world with regularity. HFMD not only causes suffering in the young and immunocompromised, but also leads to complications such as aseptic meningitis, encephalitis, poliomyelitis-like paralysis and even fatal pulmonary oedema or haemorrhage in those infected by

EV71. There is no vaccine for HFMD to date and it is of great importance to characterize the structures of $3C^{pro}$ in order to develop therapeutics for the control and treatment of HFMD. In this study, the crystal structures of EV71 $3C^{pro}$ and its complex with rupintrivir were investigated. It is shown that the structures of $3C^{pro}$ from HRV and EV71 are highly similar, especially around the active and substrate-binding sites. As a result of the similarity in structure, inhibitors developed for one enzyme can fit well into the other. Correlating with the favourable interactions, rupintrivir is highly potent against the infectivity of EV71 in a cell-based assay and against the enzymatic activity of EV71 $3C^{pro}$.

HRV causes respiratory diseases and the administration of drugs such as rupintrivir by inhalation is an effective measure. Enteroviruses take the gastrointestinal route and their infection can spread to the central nervous and other systems. Although rupintrivir is a potent compound against the activity of $3C^{pro}$, its pharmacokinetic properties should be improved for the treatment of enteroviral infections, which affect different systems through different routes compared with HRV infection; this is of particular importance in light of the fact that the bioavailability of rupintrivir is as low as 8% (Thomson Reuters Drug Report). In this work, structures of EV71 $3C^{pro}$ were characterized, setting the foundation for the improvement of compounds such as rupintrivir for the treatment of HFMD.

This work was supported by the National Basic Research Program of China (973 Program, 2012CB724500), the Open Research Fund of the State Key Laboratory of Cellular Stress Biology, Xiamen University (SKLCSB2012KF003) and the 111 Project of Education of China (B06016). The use of beamline BL17U1 at Shanghai Synchrotron Radiation Facility for crystallographic data collection is gratefully acknowledged. The able assistance of Li Fan of Wuxi Apptec Co. Ltd in the cell-based assays is also acknowledged.

## References

Birtley, J. R., Knox, S. R., Jaulent, A. M., Brick, P., Leatherbarrow, R. J. & Curry, S. (2005). *J. Biol. Chem.* **280**, 11520–11527.
Cui, S., Wang, J., Fan, T., Qin, B., Guo, L., Lei, X., Wang, J., Wang, M. & Jin, Q. (2011). *J. Mol. Biol.* **408**, 449–461.
Emsley, P., Lohkamp, B., Scott, W. G. & Cowtan, K. (2010). *Acta Cryst.* D**66**, 486–501.
Lebedev, A. A., Young, P., Isupov, M. N., Moroz, O. V., Vagin, A. A. & Murshudov, G. N. (2012). *Acta Cryst.* D**68**, 431–440.
Lu, G., Qi, J., Chen, Z., Xu, X., Gao, F., Lin, D., Qian, W., Liu, H., Jiang, H., Yan, J. & Gao, G. F. (2011). *J. Virol.* **85**, 10319–10331.
Matthews, D. A. *et al.* (1999). *Proc. Natl Acad. Sci. USA*, **96**, 11000–11007.
McCoy, A. J., Grosse-Kunstleve, R. W., Adams, P. D., Winn, M. D., Storoni, L. C. & Read, R. J. (2007). *J. Appl. Cryst.* **40**, 658–674.
Mosimann, S. C., Cherney, M. M., Sia, S., Plotch, S. & James, M. N. G. (1997). *J. Mol. Biol.* **273**, 1032–1047.
Murshudov, G. N., Skubák, P., Lebedev, A. A., Pannu, N. S., Steiner, R. A., Nicholls, R. A., Winn, M. D., Long, F. & Vagin, A. A. (2011). *Acta Cryst.* D**67**, 355–367.
Murshudov, G. N., Vagin, A. A. & Dodson, E. J. (1997). *Acta Cryst.* D**53**, 240–255.
Otwinowski, Z. & Minor, W. (1997). *Methods Enzymol.* **276**, 307–326.
Racaniello, V. R. (2006). *Picornavirdae: The Viruses and Their Replication*, 5th ed. Philadelphia: Lippincott Williams & Wilkins.
Schechter, I. & Berger, A. (1967). *Biochem. Biophys. Res. Commun.* **27**, 157–162.
Sweeney, T. R., Roqué-Rosell, N., Birtley, J. R., Leatherbarrow, R. J. & Curry, S. (2007). *J. Virol.* **81**, 115–124.
Wang, J., Fan, T., Yao, X., Wu, Z., Guo, L., Lei, X., Wang, J., Wang, M., Jin, Q. & Cui, S. (2011). *J. Virol.* **85**, 10021–10030.
Weng, K.-F., Li, M.-L., Hung, C.-T. & Shih, S.-R. (2009). *PLoS Pathog.* **5**, e1000593.
Winn, M. D. *et al.* (2011). *Acta Cryst.* D**67**, 235–242.
Yang, Y., Liang, Y., Qu, L., Chen, Z., Yi, M., Li, K. & Lemon, S. M. (2007). *Proc. Natl Acad. Sci. USA*, **104**, 7253–7258.
Yin, J., Cherney, M. M., Bergmann, E. M., Zhang, J., Huitema, C., Pettersson, H., Eltis, L. D., Vederas, J. C. & James, M. N. G. (2006). *J. Mol. Biol.* **361**, 673–686.
Zunszain, P. A., Knox, S. R., Sweeney, T. R., Yang, J., Roqué-Rosell, N., Belsham, G. J., Leatherbarrow, R. J. & Curry, S. (2010). *J. Mol. Biol.* **395**, 375–389.